ChemPubSoc Europe

DOI: 10.1002/celc.201801196

CHEMELECTROCHEM Articles

# Molten Salts Derived Copper Tungstate Nanoparticles as Bifunctional Electro-Catalysts for Electrolysis of Water and Supercapacitor Applications

Jahangeer Ahmed,*[a] Tansir Ahamad,[a] Norah Alhokbany,[a] Basheer M. Almaswari,[a] Tokeer Ahmad,[b] Afzal Hussain,[c] Eida Salman Saad Al-Farraj,[d] and Saad M. Alshehri*[a]

Herein, we report molten salts derived, cube-shaped $CuWO_4$ nanoparticles (50 ± 5 nm) as multi-functional catalysts in electrochemical and photo-electrochemical studies. The formation of pure phase cube-shaped $CuWO_4$ nanoparticles (CWO-NPs) is analyzed by X-ray diffraction, Raman spectroscopy, X-ray photoelectron spectroscopy (XPS) and field-emission electron microscopy (FE-SEM and FE-TEM). CWO-NPs show remarkable bifunctional electro-catalytic behavior for the oxygen evolution (OER) and oxygen reduction reactions (ORR) in 1.0 M KOH electrolyte solution. Polarization studies of CWO-NPs exhibit low over-potential (~260 mV) at 1 mA/cm$^2$ and low Tafel slope value (~190 mV/dec) for OER compared to bulk or other oxides. Polarization studies with controlled electrode rotation reveal a four-electron pathway for the water electrolysis reaction for OER/ORR. In addition, CWO-NPs show promising capacitive behavior with specific capacitance values of ~230 F/g using 1 M KOH electrolyte. Galvanostatic charge-discharge (GCD) studies of CWO-NPs displays low energy loss during discharge time for 50 segments. To further investigate the potential for industrial applications, the stability of the electrodes is also examined using chrono-amperometry (CA) at fixed potential, chrono-potentiometry (CP) at fixed current density, and cyclic voltammetry (CV) with 50 cycles.

## 1. Introduction

Electrolysis of water has received interest in sustainable, renewable, clean, and alternative energy resources via hydrogen evolution, oxygen evolution, and oxygen reduction reactions (HER, OER and ORR). Hence, the efficiency of electrolysis of water can be determined by measuring the electro-activities of the materials to HER, OER and ORR. Till now, noble metals (Ru, Ir, Pt etc.) and their oxides are the most efficient electro-active materials for HER, ORR and ORR,[1] but their immense cost and scarcity nature make them limited for commercialization. Supercapacitors have fascinated an attention for energy storage through adsorption-desorption charge storage at the surface of electrodes. Commercially available noble metal based supercapacitors (e.g. $RuO_2$) do not meet to high energy demand worldwide due to their short life and slow charge-discharge capacity.[2] Therefore, the researchers are motivated to explore naturally abundant low cost electro-active materials to replace the high cost noble metals or their oxides catalysts for energy conversion and storage. Copper based tungstate materials are earth abundant and cost-effective electrodes for clean, renewable and sustainable energy devices compared to expensive noble metal electrodes.

Nanoscrystalline metal tungstate particles were considered as effective catalysts for electrolysis of water and supercapacitors.[3,4] A wide over-potential range of these metal tungstate particles was reported for electrolysis of water.[3] High over-potential and Tafel values may destroy the stability of the catalysts and to reduce the electro-catalytic performances. Therefore, the electrode materials with low over-potential and Tafel values have potential to enhance the electrochemical performances. Dhilip Kumar et al. have reported that $CuWO_4$ nanoparticles could be promising in supercapacitors, and the specific capacitance (Cs) of these nanoparticles was reported of ~15 F/g with scan rate of 5 mV/s in 2 M KOH electrolyte.[5] Zinc and nickel tungstate nanomaterials have also shown supercapacitive nature with the Cs values of ~72 F/g (3 M KOH)[6] and ~171 F/g (2 M KOH)[7] respectively. Copper tungstate nanoparticles were reported as efficient catalysts for photo-electrochemical water oxidation reactions[8,9] and sensing applications.[10] Besides, nanocrystalline $CuWO_4$ materials were used as the photo-catalysts in the degradation of organic pollutants from aqueous through sunlight irradiation.[11] To the best of our knowledge; only one report is found in literature regarding supercapacitors based on $CuWO_4$, while electrolysis of water by

[a] J. Ahmed, T. Ahamad, N. Alhokbany, B. M. Almaswari, S. M. Alshehri
Department of Chemistry
College of Science
King Saud University
Riyadh 11451, Saudi Arabia
E-mail: jahmed@ksu.edu.sa
alshehri@ksu.edu.sa
[b] T. Ahmad
Nanochemistry Laboratory, Department of Chemistry, Jamia Millia Islamia, New Delhi 110025, India
[c] A. Hussain
Department of Pharmacognosy
College of Pharmacy
King Saud University
Riyadh 11451, Saudi Arabia
[d] E. S. S. Al-Farraj
Al Imam Mohammad Ibn Saud Islamic University (IMSIU)
College of Sciences
Department ofChemistry
11623 Riyadh, Saudi Arabia

$CuWO_4$ has not been reported till yet. We believe that $CuWO_4$ nanostructures have great interest in electrolysis of water for renewable and clean energy sources. Therefore, we have motivated to prepare $CuWO_4$ nanostructured materials to study their electro-chemical activities at room temperature. Recently, we have reported various mixed metal oxide nanostructures for photo-catalysis,[12] electro-catalysis,[13,14] and supercapacitors.[15]

Herein, we report ecofriendly and low cost molten salts synthesis of cube-shaped $CuWO_4$ nanoparticles (CWO-NPs) as the promising catalysts for electrolysis of water and super-capacitors. CWO-NPs were characterized by powder X-ray diffraction, FTIR, Raman, field emission electron microscopy (FE-SEM and FE-TEM), XPS, BET surface area, and energy dispersive (EDAX) studies. Electrochemical studies of CWO-NCs were carried out in details using cyclic voltammetry, linear sweep voltammetry with rotating disk electrode, and chronoamperometry in alkaline medium. The specific capacitances (Cs) and galvanostatic charge – discharge studies were carried out for super-capacitive performance of CWO-NPs. Optical and photo-electrochemical properties were also investigated.

## Experimental Section

$Cu(NO_3)_2.3H_2O$ (BDH, 98%), $Na_2WO_4.2H_2O$ (BDH, 96%), $NaNO_3$ (Alfa Aesar, 98 + %) and $KNO_3$ (Alfa Aesar, 99%) chemicals were taken in 1:1:45:45 molar ratio, respectively. The above mixture was ground together for 30 minutes in an agate mortar-pestle, and then transferred in to the crucible followed by firing at 500 °C / 6 h. The resulting products were washed by DI water several times and then dried at 60 °C for overnight. The final product was grey in color. Note that the firing temperature of the mixture was fixed on the basis of reported phase diagram of $NaNO_3$ and $KNO_3$ salts.[16] This is very simple, low cost, and ecofriendly procedure for the synthesis of the nanostructured materials.[17] Excess amount of molten salts works as solvent and plays an important role for controlling the morphology (size and shape) of the nanomaterials by transmitting the energy to the precursor system. Phase purity of CWO-NPs was characterized by powder X-ray diffraction (PXRD, Rigaku MiniFlex, Ni-filtered Cu–Kα radiation), FTIR (Bruker TENSOR 27 Spectrometer) and Raman spectroscopy (Renishaw instrument with Ar-laser source of 488 nm). Morphological studies were carried out on field emission electron microscopy (FESEM: JEOL JSM-7600F at 5 kV and HRTEM: JEOL JSM-2100F at 200 kV). BET surface area of CWO-NPs was recorded on V-Sorb-2800-Porosimetry (Gold APP-Instruments, China). XPS data was recorded on Kratos AxisUltra DLD electron spectrometer at the base pressure of 40000 torr (PHI 5300). Optical data of CWO-NPs was recorded on a UV-vis spectrophotometer (UV-1650, SHIMADZU).

Electrochemical characterization of CWO-NPs were accomplished on potentiostat – galvanostat electrochemical analyzer (CHI 660E, China) at room temperature. For the electrolysis of water; the working electrodes were prepared by pasting of one drop of slurry on the glassy carbon electrode. The procedure of slurry preparation is given elsewhere.[13] The loaded mass of CWO-NPs catalysts was ~0.24 mg/cm$^2$ on GC electrode (0.07 cm$^2$). Pt-wire and Ag/AgCl electrodes were used as counter and reference electrode, respectively, in water electrolysis reactions. The Nernst equation (E(RHE) = E(Ag/AgCl) + 0.059 pH + 0.197 V at 25 °C) can be used to convert the potential of Ag/AgCl reference electrode to RHE (reversible hydrogen electrode).[13] For the supercapacitors; the working electrode was prepared by pasting the slurry on carbon paper (1 mg/cm$^2$) containing the weight fraction of 75:15:10 of CWO-NPs catalysts: carbon black: PVDF. The working electrodes for super-capacitors were dried at 60 °C/24 h. The galvanostatic charge-discharge (GCD) measurements were done for 50 segments. The stability tests of CWO-NCs electrodes were also examined by chronoamperometry (CA) at fixed potential, chronopotentiometry (CP) at fixed current density and CVs at 50 cycles.

A photo-electrode for photo-electrochemical reaction has been prepared. 27 mg of CWO-NPs with 10 ml ethanol were sonicated for 5 minutes to make the suspension. One ml of the suspension was mixed with 8 ml of ethanol and then sonicated again for 5 minutes. An ITO electrode (2 cm × 1 cm) was dipped in the above resulting suspension and left for overnight. Thereafter, the super-natant solution was removed carefully and then the photo-electrode was dried in oven at 70 °C for 3 h. Photo-electrochemical reactions were carried out in a PEC cell and the photocurrent was recorded on a potentiostat–galvanostat electrochemical (i.e. three electrode) work station. An ozone-free xenon lamp (450 W) was used as the light source and potassium phosphate buffer (pH = 7) was used as an electrolyte in photo-electrochemical reaction

## 2. Results and Discussion

Powder X-ray diffraction (PXRD) studies of CWO-NCs were shown in Figure 1a. PXRD patterns show well crystalline nature of pure phase of cube-shaped $CuWO_4$ nanoparticles, which perfectly indexed with triclinic structure of $CuWO_4$ (JCPDS file # 01-080-1918). Figure 1b shows FTIR spectrum of CWO-NPs. The IR bands at ~3440 and ~1630 cm$^{-1}$ arise due to presence of moisture (–OH group). Presence of IR bands at ~2347 and ~1385 cm$^{-1}$ could be due to the atmospheric carbon dioxide. The characteristics IR bands, in the range from 471 to 901 cm$^{-1}$, can be attributed to the formation of $CuWO_4$ phase as also reported previously.[18] Figure 1c represents Raman spectrum of CWO-NPs. We have observed the strongest Raman band at ~902 cm$^{-1}$ which could be attributed to symmetric stretching vibration (ν1) of W–O bond (Ag). The peak observed at ~305 cm$^{-1}$ could be attributed to ν2 vibration (Ag) of tungstate. The peak at ~771 cm$^{-1}$ belongs to ν2 vibration (Eg) of W–O. The band at ~392 cm$^{-1}$ could be assigned to Ag modes of W–O. The remaining bands were also indexed and could be assigned to Ag mode of Raman active modes as also reported in literature.[19] All Raman active vibrational modes can be recognized on the basis of triclinic structure of $CuWO_4$, which is in good agreement with previously reported work of Raman modes of $CuWO_4$.[19,20] Note that small dislocations of peak positions were observed, which could be due to slight variations in degree of structural order/disorder of $WO_6$ and $CuO_6$ based on the synthetic method and parameters of the prepared materials. BET surface area of CWO-NPs was investigated using $N_2$ adsorption–desorption isotherm as shown in Figure 1d. Surface area of CWO-NPs was found to be ~12.20 m$^2$/g which nearly consistent with previous reports at similar firing conditions.[21]

Field emission SEM and TEM studies were supported to the shape and size of cube-shaped $CuWO_4$ nanoparticles. Figure 2a shows low magnification FE-SEM micrograph of $CuWO_4$, which reveals the formation of particles in nanometric region. Energy

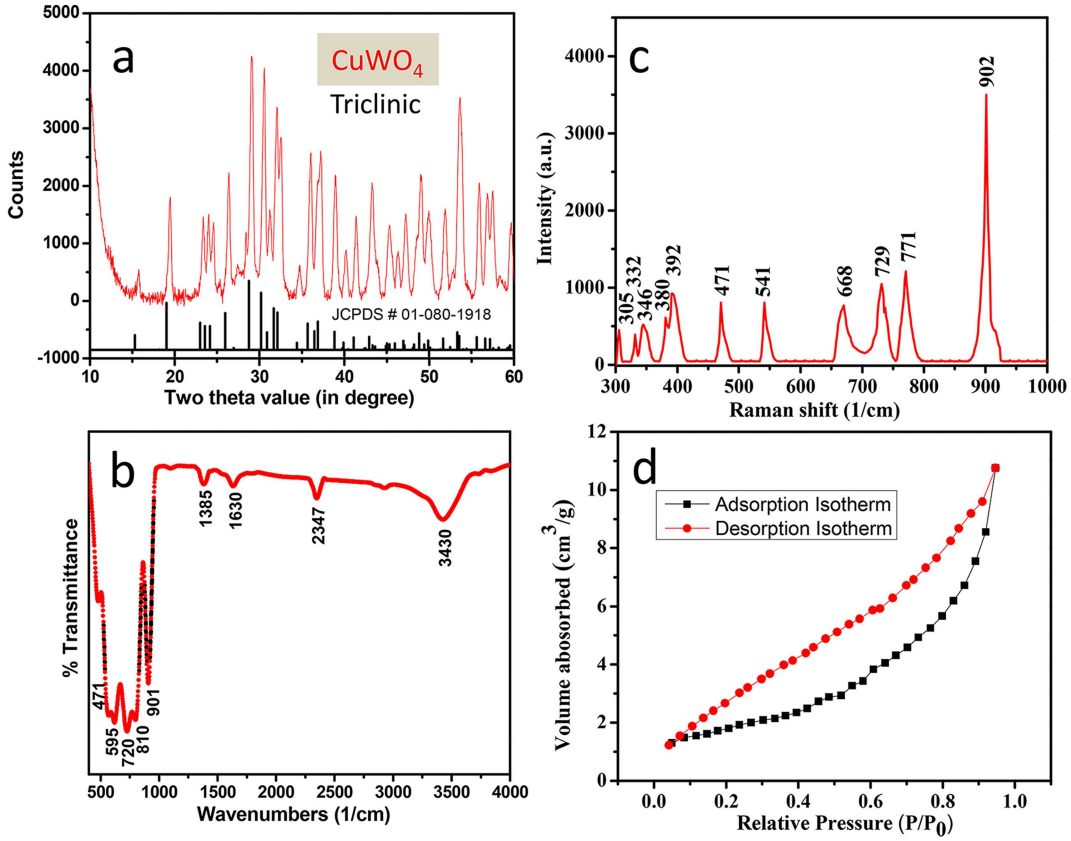


**Figure 1.** a) PXRD, b) FTIR, c) Raman, and d) $N_2$ adsorption–desorption isotherm of CWO-NPs.

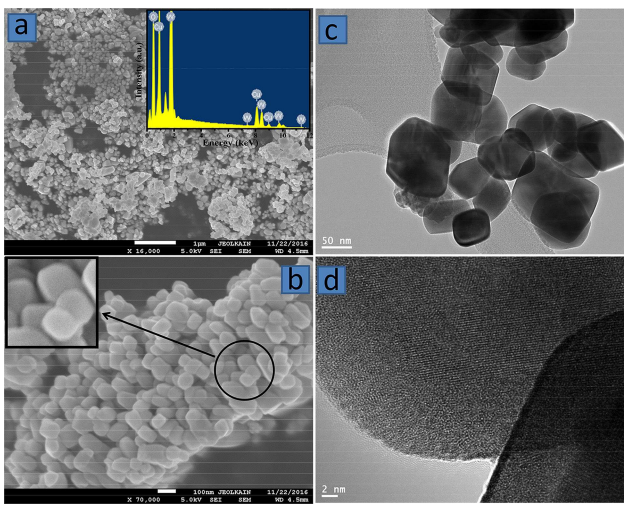


**Figure 2.** a) Low magnification FE-SEM, b) high magnificcation FE-SEM, c) FE-TEM, and d) High resolution FE-TEM micrographs of CWO-NPs. Inset of Figure (a) and (b) show EDAX and closer view of FESEM image of CWO-NPs.

dispersive X-ray studies (equipped with FE-SEM) of the nanoparticles confirmed the presence of copper and tungsten elements. The elemental composition (atomic weight%) was fairly similar to the initial loaded stoichiometry of the constituents (inset of Figure 2a). Figure 2b represents high magnification FE-SEM micrograph of the resulted nanoparticles. A careful visualization of microscopic studies confirms the formation of cube – shaped nanoparticles of $CuWO_4$ as shown in inset of Figure 2b. FE-SEM based morphological studies of CWO-NPs are strongly supported by FE-TEM. The average size of cube-shaped nanoparticles was found to be ~50 nm from FETEM studies (Figure 2c). High resolution FE-TEM studies illustrate the crystalline nature of CWO-NPs (Figure 2d).

Figure 3a shows the XPS spectra of $CuWO_4$ for the confirmation of the presence of elements (Cu, W, and O) and their oxidation state. A core-level spectrum of W (4f) shows the binding energies of W($4f_{7/2}$), and W($4f_{5/2}$) at 35.24, and 37.31 eV, respectively, which is in good agreement with the standard data for $W^{6+}$ (Figure 3b). The core-level spectrum of Cu (2p) has been shown in Figure 3c. The binding energies of Cu($2p_{3/2}$) and Cu($2p_{1/2}$) at 934.12 and 954.01 eV, respectively, resemble to bivalent oxidation state of copper (Figure 3c). In addition, we observed two strong peaks at 943.12 and 962.84 eV of $Cu^{2+}$ state, which proved by a process involving motivation of electrons from the valence band to conduction band, resulting in producing a 2p vacancy. Figure 4d shows the high-resolution spectrum of O (1 s), which could be deconvoluted into two peaks at the binding energies of 528.90 eV and 531.42 eV corresponding to Cu–O and W–O–W bonds respectively. These XPS results confirm that the prepared material is pure $CuWO_4$ without any impurities, which is also in good agreement with the previous reports.[22]

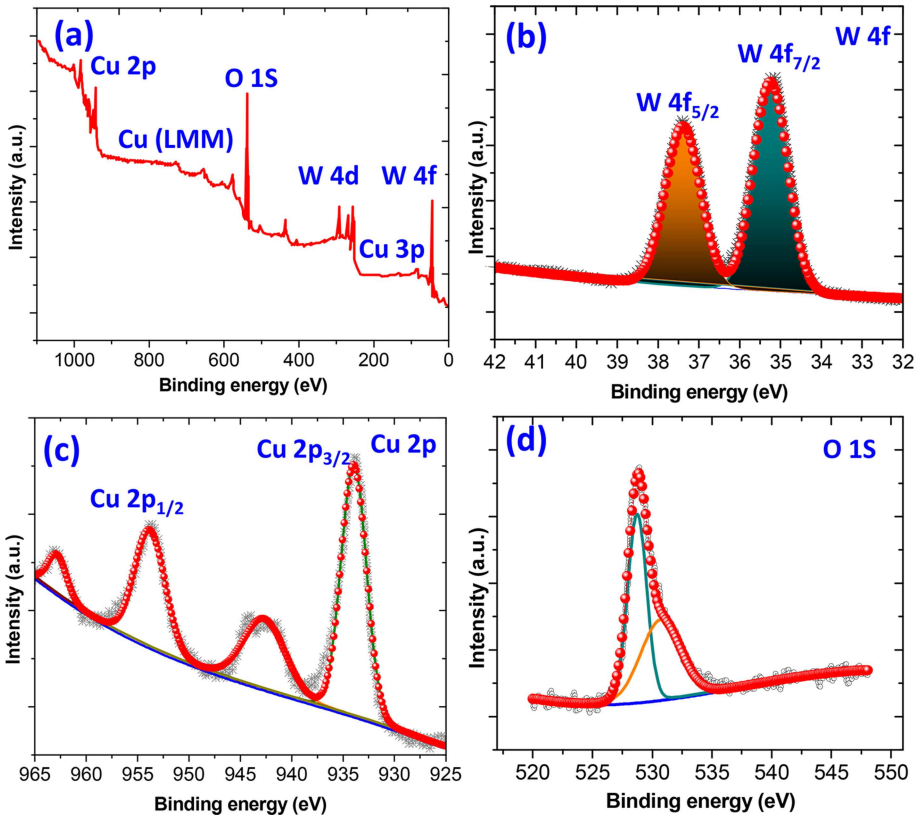


**Figure 3.** a) XPS spectra of $CuWO_4$. High-resolution XPS spectra of b) W4f, c) Cu 2p, d) O 1s.

Electrolysis of water (OER and ORR) was carried out in alkaline medium using CWO-NPs catalysts as electro-active electrode materials. Cathodic and anodic scans of cyclic voltammetry (CV) show bifunctional redox behavior of CWO-NPs to ORR/ OER in the potential window from −1 to +1 V versus Ag/AgCl at the scan rate of 50 mV/s using 1 M KOH electrolyte (Figure 4a). Linear sweep polarization (LSP) curves confirm OER and ORR via electrolysis. Figure 4b shows LSP curve of CWO-NPs in potential range from 0.0 to 1.0 V (anodic region) for OER at 50 mV/s scan rate. The onset potential and the current density of CWO-NPs are recorded to be ~0.48 V and ~20 mA/cm$^2$ for OER. The over-potentials of the electrodes for OER were found to be ~260 mV ( $\eta_1$) and ~570 mV ($\eta_{10}$) at 1 and 10 mA/cm$^2$ respectively. $\eta_1$ and $\eta_{10}$ are denoted as the over-potentials at the current densities of 1 and 10 mA/cm$^2$, respectively, and the values of $\eta_1$ and $\eta_{10}$ are calculated by the abstraction of water oxidation potential. Determination of over-potential of electro-catalysts is reported elsewhere.[23] A linearly fitted Tafel plot of CWO-NPs for OER is given in inset of Figure 4b. Tafel slope of CWO-NPs is found to be ~190 mV/ decade. Current values of over-potential and Tafel slop for OER (i.e. oxidation reaction) were comparatively lower than previous reports of other oxides. Low over-potentials and tafel values of the electro-catalysts sustain high stability and high current with low energy loss during water redox reactions. Polarization studies for ORR were carried out in cathodic region by applying the potential range from 0.0 to − 0.8 V using rotating disk electrodes (RDE) at 10 mV/s (Figure 4c). The rotation speed of the electrode was limited from 500 to 3000 rpm. We observed that the diffusion current densities of CWO-NPs increase with rotations. This could be done due to oxygen diffusion distance. Thereafter, we have employed a Koutecky–Levich (K–L) equation[24] to investigate the kinetics of water redox reaction (Figure 4d). We have analyzed K–L plots ($J^{-1}$ versus $\omega^{-1/2}$) at various potentials to estimate the number of electrons (n) transferred. The transferred electrons in electrolysis was found to be in the range from 3.92–4.04 (i.e. ~4 e−) in potentials range from −0.5 to −0.75 V using Ag/AgCl reference electrode. Linearly fitted slopes confirm the first order reaction of oxygen reduction. The present values are in good agreement with literature of $NiCo_2O_4$/C and commercial Pt/C.[25] The following K–L equation has been used to calculate the number of electrons (*n*):

$$\frac{1}{J} = \frac{1}{J_L} + \frac{1}{J_k} = \frac{1}{B\omega^{1/2}} + \frac{1}{J_k}$$

$$B = 0.62\, nFC_o(D_o)^{2/3}\nu^{-1/6}$$

$$J_k = nFkC_o$$

Where; J = current density (A cm$^{-2}$), $J_K$ = kinetic current density (A cm$^{-2}$), JL = diffusion-limiting current densities (A cm$^{-2}$), F = Faraday's constant, $D_o$ = diffusion coefficient of $O_2$ in 1.0 M KOH, ν = kinematic viscosity of electrolyte, $C_o$ = saturation concentration of $O_2$, and ω = rotation rate.

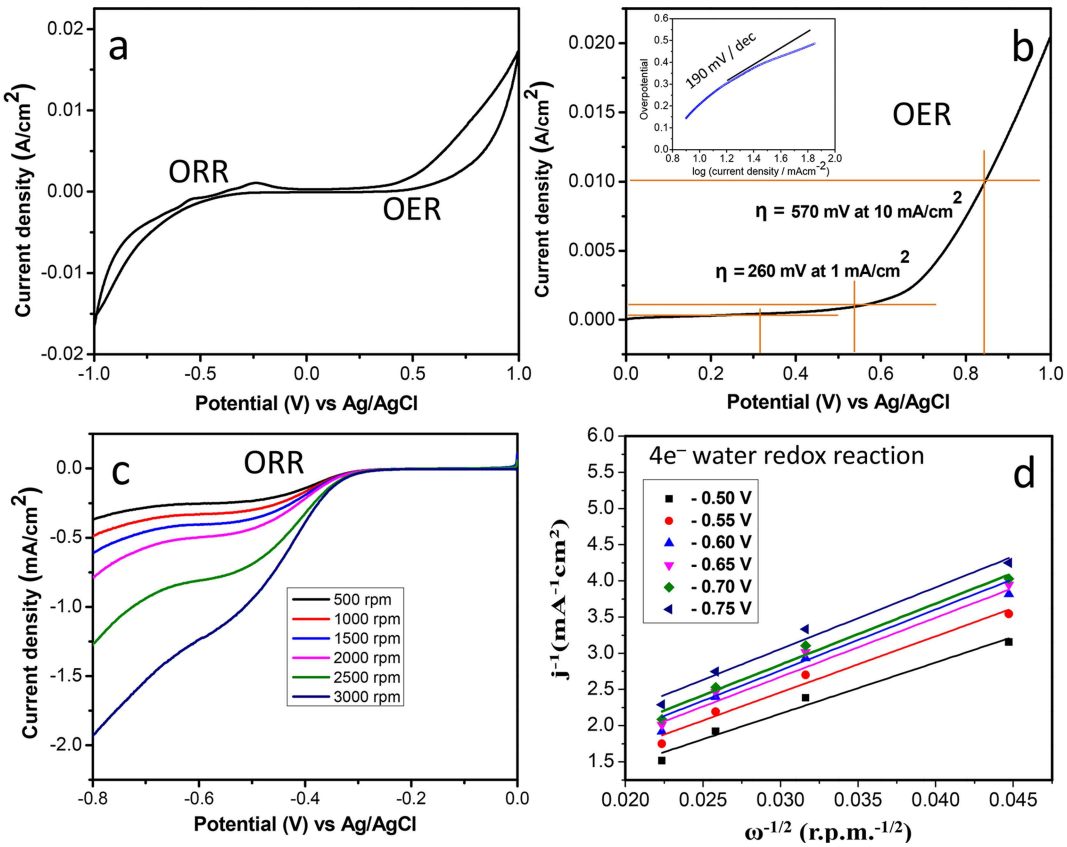


**Figure 4.** a) CV for OER/ORR, b) LSV for OER, c) LSV for ORR, and d) K–L plots of CWO-NPs for electrolysis of water in 1.0 M KOH. Inset of Figure 3b represents Tafel plot.

The oxygen evolution and oxygen reduction reactions were occurred at the surface of electrode in anodic and cathodic regions, respectively, in alkaline medium as given: $4OH^- \rightarrow O_2 + 4e^- + 2H_2O$ (For OER) and $O_2 + 4e^- + 2H_2O \rightarrow 4OH^-$ (For ORR). Figure 5 shows the CV curves of CWO-NPs for ORR in oxygen saturated system and absence of oxygen for cathodic sweeps. CV curves clearly show the oxygen reduction reaction in presence of oxygen saturated system while no oxygen reduction reaction was observed in absence of oxygen. Note that all the dissolved oxygen was removed by purging the nitrogen gas throughout the electrolyte solution prior to run the CV measurement in absence of oxygen.

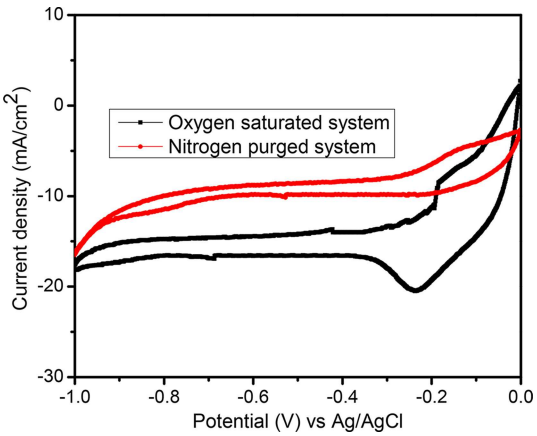


**Figure 5.** CVs of CWO-NPs for ORR in presence and absence of oxygen in 1 M KOH.

Supercapacitor performance of CWO-NPs was also investigated in 1 M KOH at the scan rate from 5 to 100 mV/s. The specific capacitance (Cs) of CWO-NPs electrode was calculated with the help of the given equation: $Cs = [(\int I(V)dv)/(vm\Delta V)]$. The terms Cs, $\int I(V)dv$, m, $v$, and $\Delta V$ represent specific capacitance (F/g), integrated area within CV curve, mass of the catalysts (g), scan rate ($mVs^{-1}$), and applied voltage window respectively. Figure 6a shows CV curves of CWO-NPs electrodes at 5, 10, 20, 50 and 100 mV/s within potential window from −0.2 to + 0.45 V vs Ag/AgCl. CV studies demonstrate efficient charge storage capacity of CWO-NPs electrode materials through faradaic redox reaction. CWO-NPs electrodes provide sufficient integrated area within CVs that illustrates high energy storage behavior of CWO-NPs electrode materials. This is noteworthy that the peak current increases with scan rate that is a good agreement of capacitive performance and rate ability of CWO-NPs electrode materials. The specific capacitance of CWO-NCs (~230 F/g at 5 mV/s in 1 M KOH) was found higher than $CuWO_4$ (10 F/g), $ZnWO_4$ (70 F/g), and $NiWO_4$ (~171 F/g) supercapacitors.[5–7] The specific capacitance values of graphene/ZnO (60–120 F/g)[26,27] and graphene/$SnO_2$ (42 F/g)[27] nanocomposite materials were reported lower than that of present result, while Au/$MnO_2$

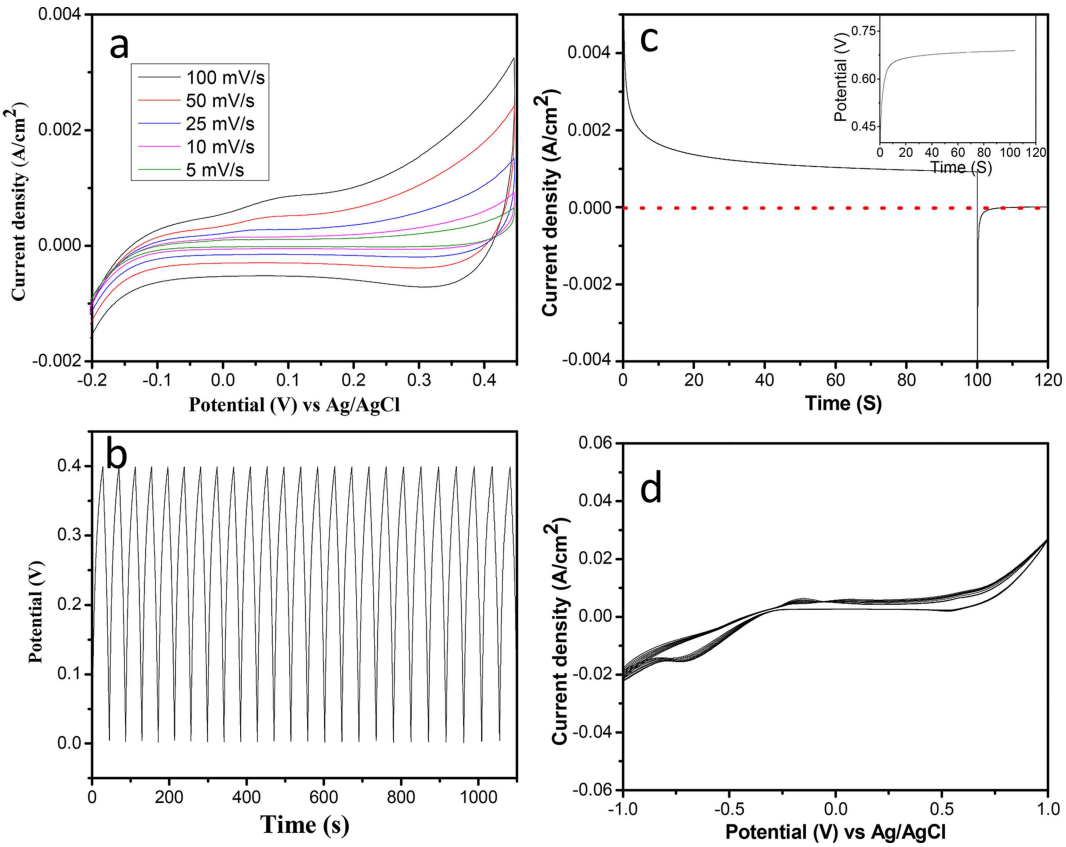


**Figure 6.** a) CV curves at the scan rate range from 5 to 100 mV/s, and b) galvanostatic charge – discharge (GCD) curves for IR drops in 50 segments of CWO-NPs. Stability tests of CWO-NPs using c) chronoameprometry and d) long term CVs for 50 cycles. Inset of Figure 5c shows chronopotentiometry of CWO-NPs.

nano-hybrid had reported much higher specific capacitance (~ 1145 F/g) than CWO-NPs.[28]

Galvanostatic charge – discharge (GCD) studies of CWO-NPs were also carried for IR drops in the potential window of 400 mV for 50 segments. Figure 6b shows GCD curves between potential (V) versus time (t). GCD measurements were accomplished at current density of 10 mA/g. GCD curves of CWO-NPs show consistent reversible cycles via charge-discharge path for 50 segments. Remarkably, very low IR drops were observed during discharge process. A small IR drop of CWO-NPs is a good sign for low interfacial resistance and energy losses. The discharge time of CWO-NPs is recorded of ~1100 seconds for 50 segments at 10 mA/g, which is directly related to high performance of the specific capacitance of CWO-NPs. The stability of the electrode materials is an important concern. Therefore, we have conducted the stability tests of CWO-NPs electrodes using chronoameprometry, chronopotentiometry, and CVs. Chronoamerometry (CA) was carried out at the fixed potential of 0.65 V for 100 seconds (Figure 6c) and similarly chronopotentiometry (CP) test was conducted at the resulted current density (from CA) for 100 seconds (inset of Figure 6c). CA and CP results confirm that CWO-NPs electrodes show stable nature for the electrochemical studies. Additionally, the stability of CWO-NPs was studied using CV for 50 cycles at 25 mV $s^{-1}$ in 1.0 M KOH (Figure 6d), which is consistent with the results obtained from CA and CP measurements. We believe that present studies could have a significance impact over precious electrode materials in electrochemically energy conversion and storage process.

We have treated CWO-NPs with 1 M KOH and washed with DI water followed by drying in oven at 60 °C. The treated powder samples were then analyzed by PXRD, SEM and TEM studies in order to check the stability of nanostructured materials in alkaline conditions. Figure 7a shows PXRD patterns of the treated powder sample, which confirm the stability of crystal structure and phase purity of CWO-NPs. Figure 7b and 7c show SEM and TEM micrographs of the treated powder samples of CWO-NPs. The slight agglomeration of the nanoparticle was observed which could be possible due to the base treatment of CWO-NPs.

UV-visible absorption measurements were carried out to study the optical properties of CWO-NPs at 25 °C. The absorbance spectrum of CWO-NPs shows a peak at ~345 nm (Figure 8a). The direct band gap of CWO-NPs was determined from the absorption data using Tauc's model. Figure 8b shows a plot of band gap energy vs $(\alpha h\nu)^2$ of CWO-NPs. Where; $\alpha$, h and $\nu$ are denoted to absorbance, Planck's constant and frequency respectively. The direct band gap of CWO-NPs was found to $3.5 \pm 0.10$ eV which is consistent with the earlier reports.[9] The direct and indirect band gaps of $CuWO_4$ were reported of 3.5 and 2.3 eV respectively.[9] The photo-electrochemical water oxidation of CWO-NPs was investigated at

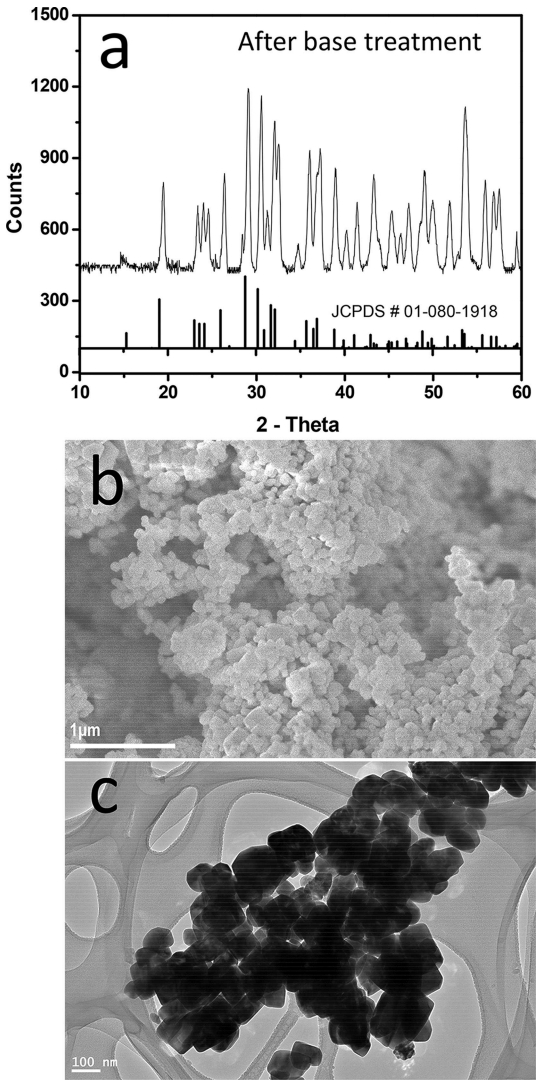


**Figure 7.** a) PXRD, b) SEM, and c) TEM studies for stability check after base treatment of CWO-NPs.

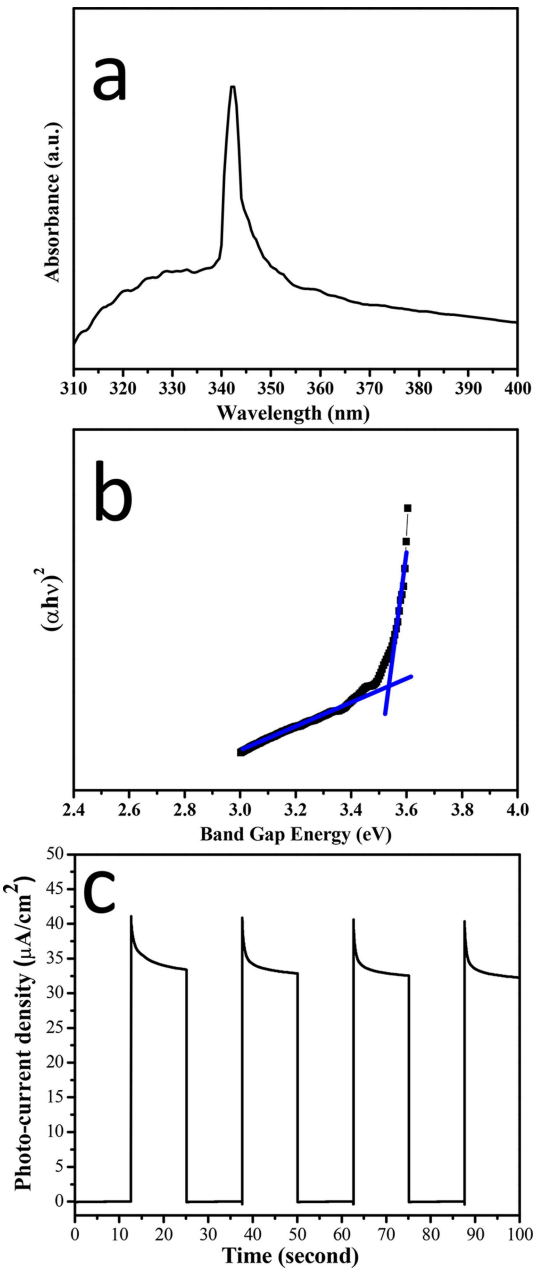


**Figure 8.** a) UV – visible, and b) direct band gap energy plots of CWO-NPs. c) Chronoamperometry of CWO-NPs photo-anode for photo-electrochemical water oxidation reaction.

0.207 V vs Ag/AgCl in potassium phosphate buffer solution (Figure 8c). An anodic photocurrent density of CWO-NPs was recorded of ~32 μA/cm$^2$ from the chronoamperometry. The photocurrent density generated in individual cycle was nearly consistent. Our result is in good agreement with previously reported photocurrent of $CuWO_4$.[9] The photo-electrochemical reaction stops and the photocurrent density of the photo-anode drop to zero, when light source was intermitted. This could be originated from the hole diffusion at the surface of photo-anode/electrolyte interface in photo-electrochemical water oxidation reaction.

## 3. Conclusions

Molten salts derived cube-shaped $CuWO_4$ nanoparticles (50 ± 5 nm) were used as multifunctional electrode materials for water electrolysis (OER/ORR), supercapacitors and photo-anode. Polarization studies of CWO-NPs were shown low over-potentials (~260 mV) and low Tafel values (~190 mV/dec) in water oxidation reactions. Polarization experiments with controlled rotation of rotating disk electrode confirmed 4 electrons system of water electrolysis. Furthermore, CWO-NPs were shown promising super-capacitive nature with Cs value of ~230 F/g at 5 mV/s. GCD measurements confirmed very low energy losses during discharge time for 50 segments. CA, CP and CVs measurements were also conducted to confirm the stability of CWO-NPs electrode materials.

## Acknowledgement

*The authors extend their sincere appreciation to the Deanship of Scientific Research at King Saud University for funding this Research Group (RG-1435-007). The researchers acknowledge the Deanship of Scientific Research at Al Imam Mohammad Ibn Saud Islamic University, Saudi Arabia, for financing this project under the grant no (381221).*

## Conflict of Interest

The authors declare no conflict of interest.

**Keywords:** $CuWO_4$ · electrocatalysis · nanoparticles · oxygen reduction · supercapacitors

[1] T. Audichon, T. W. Napporn, C. Canaff, C. Morais, C. Comminges, K. B. Kokoh, *J. Phys. Chem. C* **2016**, *120*, 2562–2573; Y. Lee, J. Suntivich, K. J. May, E. E. Perry, Y. Shao-Horn, *J. Phys. Chem. Lett.* **2012**, *3*, 399–404; J. Ahmed, Y. Mao, *Electrochim. Acta* **2016**, *212*, 686–693; T. Reier, M. Oezaslan, P. Strasser, *ACS Catal.* **2012**, *2*, 1765–1772; K. Eid, H. Wang, V. Malgras, S. M. Alshehri, T. Ahamad, Y. Yamauchi, L. Wang, *J. Electroanal. Chem.* **2016**, *779*, 250–255.

[2] F. Pico, J. Ibañez, M. A. Lillo-Rodenas, A. Linares-Solano, R. M. Rojas, J. M. Amarilla, J. M. Rojo, *J. Power Sources* **2008**, *176*, 417–425.

[3] H. Jia, J. Stark, L. Q. Zhou, C. Ling, T. Sekito, Z. Markin, *RSC Adv.* **2012**, *2*, 10874–10881; C. Ling, L. Q. Zhou, H. Jia, *RSC Adv.* **2014**, *4*, 24692–24697; V. K. V. P. Srirapu, A. Kumar, P. Srivastava, R. N. Singh, A. S. K. Sinha, *Electrochim. Acta* **2016**, *209*, 75–84.

[4] S. Chen, G. Yang, Y. Jia, H. Zheng, *ChemElectroChem* **2016**, *3*, 1490–1496; K. Ding, X. Zhang, J. Li, P. Yang, X. Cheng, *ChemElectroChem*, n/a; G. He, J. Li, W. Li, B. Li, N. Noor, K. Xu, J. Hu, I. P. Parkin, *J. Mater. Chem. A* **2015**, *3*, 14272–14278.

[5] R. Dhilip Kumar, Y. Andou, M. Sathish, S. Karuppuchamy, *J. Mater. Sci. Mater. Electron.* **2016**, *27*, 2926–2932.

[6] S. R. Ede, A. Ramadoss, U. Nithiyanantham, S. Anantharaj, S. Kundu, *Inorg. Chem.* **2015**, *54*, 3851–3863.

[7] R. D. Kumar, Y. Andou, S. Karuppuchamy, *J. Alloys Compd.* **2016**, *654*, 349–356.

[8] A. E. B. Lima, M. J. S. Costa, R. S. Santos, N. C. Batista, L. S. Cavalcante, E. Longo, G. E. Luz, *Electrochim. Acta* **2017**, *256*, 139–145; S. Kannan, K. Mohanraj, G. Sivakumar, *ChemistrySelect* **2017**, *2*, 4484–4498; Y. Gao, T. W. Hamann, *Chem. Commun.* **2017**, *53*, 1285–1288; Y. Gao, T. W. Hamann, *J. Phys. Chem. Lett.* **2017**, *8*, 2700–2704; W. Ye, F. Chen, F. Zhao, N. Han, Y. Li, *ACS Appl. Mater. Interfaces* **2016**, *8*, 9211–9217; J. E. Yourey, B. M. Bartlett, *J. Mater. Chem.* **2011**, *21*, 7651–7660.

[9] D. J. Jovanovic, I. V. M. Mitric, J. M. Nedeljkovic, *Acta Chim. Slov.* **2012**, *59*, 70–74; M. Davi, A. Drichel, M. Mann, T. Scholz, F. Schrader, A. Rokicinska, P. Kustrowski, R. Dronskowski, A. Slabon, *J. Phys. Chem. C* **2017**, *121*, 26265–26274.

[10] K. Aneesh, C. S. R. Vusa, S. Berchmans, *Sens. Actuators B* **2017**, *253*, 723–730; L. Wang, A. U. Rehman, H. Wu, B. Wu, L. Li, K. Shi, *RSC Adv.* **2016**, *6*, 69999–70007.

[11] Z. Barzgari, S. Z. Askari, A. Ghazizadeh, *J. Mater. Sci. Mater. Electron.* **2017**, *28*, 3293–3298; H. Chen, X. Xiong, L. Hao, X. Zhang, Y. Xu, *Appl. Surf. Sci.* **2016**, *389*, 491–495; L. Liang, H. Liu, Y. Tian, Q. Hao, C. Liu, W. Wang, X. Xie, *Mater. Lett.* **2016**, *182*, 302–304; X. Xie, M. Liu, C. Wang, L. Chen, J. Xu, Y. Cheng, H. Dong, F. Lu, W.-H. Wang, H. Liu, W. Wang, *RSC Adv.* **2016**, *6*, 953–959; D. P. Dutta, A. Rathore, A. Ballal, A. K. Tyagi, *RSC Adv.* **2015**, *5*, 94866–94878.

[12] S. M. AlShehri, J. Ahmed, T. Ahamad, B. M. Almaswari, A. Khan, *J. Nanopart. Res.* **2017**, *19*, 289; S. M. AlShehri, J. Ahmed, A. M. Alzahrani, T. Ahamad, *New J. Chem.* **2017**, *41*, 8178–8186.

[13] S. M. AlShehri, J. Ahmed, T. Ahamad, P. Arunachalam, T. Ahmad, A. Khan, *RSC Adv.* **2017**, *7*, 45615–45623.

[14] J. Ahmed, V. V. Poltavets, J. Prakash, S. M. Alshehri, T. Ahamad, *J. Alloys Compd.* **2016**, *688*, Part A, 1157–1161.

[15] S. M. Alshehri, J. Ahmed, A. N. Alhabarah, T. Ahamad, T. Ahmad, *ChemElectroChem* **2017**, *4*, 2952–2958.

[16] C. M. Kramer, C. J. Wilson, *Thermochim. Acta* **1980**, *42*, 253–264.

[17] Y. Mao, T.-J. Park, F. Zhang, H. Zhou, S. S. Wong, *Small* **2007**, *3*, 1122–1139; H. Zhou, Y. Mao, S. S. Wong, *J. Mater. Chem.* **2007**, *17*, 1707–1713.

[18] S. M. Pourmortazavi, M. Rahimi-Nasrabadi, Y. Fazli, M. Mohammad-Zadeh, *Int. J. Refract. Met. Hard Mater.* **2015**, *51*, 29–34.

[19] A. E. B. Lima, M. J. S. Costa, R. S. Santos, N. C. Batista, L. S. Cavalcante, E. Longo, G. E. Luz, *Electrochim. Acta* **2017**, *256*, 139–145.

[20] E. L. S. Souza, J. C. Sczancoski, I. C. Nogueira, M. A. P. Almeida, M. O. Orlandi, M. S. Li, R. A. S. Luz, M. G. R. Filho, E. Longo, L. S. Cavalcante, *Ultrason. Sonochem.* **2017**, *38*, 256–270.

[21] H. Chen, Y. Xu, *RSC Adv.* **2015**, *5*, 8108–8113.

[22] Y. Tang, N. Rong, F. Liu, M. Chu, H. Dong, Y. Zhang, P. Xiao, *Appl. Surf. Sci.* **2016**, *361*, 133–140; O. Y. Khyzhun, T. Strunskus, S. Cramm, Y. M. Solonin, *J. Alloys Compd.* **2005**, *389*, 14–20.

[23] A. M. Appel, M. L. Helm, *ACS Catal.* **2014**, *4*, 630–633.

[24] R. Zhou, Y. Zheng, M. Jaroniec, S.-Z. Qiao, *ACS Catal.* **2016**, *6*, 4720–4728; Z. Wu, W. Li, Y. Xia, P. Webley, D. Zhao, *J. Mater. Chem.* **2012**, *22*, 8835–8845.

[25] J. Wang, Z. Wu, L. Han, R. Lin, H. L. Xin, D. Wang, *ChemCatChem* **2016**, *8*, 736–742.

[26] M. Saranya, R. Ramachandran, F. Wang, *J. Adv. Mater.* **2016**, *1*, 454–460.

[27] T. Lu, Y. Zhang, H. Li, L. Pan, Y. Li, Z. Sun, *Electrochim. Acta* **2010**, *55*, 4170–4173.

[28] X. Lang, A. Hirata, T. Fujita, M. Chen, *Nature* **2011**, *6*, 232.

Manuscript received: August 29, 2018
Accepted Article published: September 25, 2018
Version of record online: October 17, 2018